Aalborg Universitet

AALBORG UNIVERSITY

DENMARK

Optics of multiple grooves in metal

transition from high scattering to strong absorption

Skjølstrup, Enok Johannes Haahr; Søndergaard, Thomas; Pedersen, Kjeld; Pedersen, Thomas Garm

Published in:
Journal of Nanophotonics

DOI (link to publication from Publisher):
10.1117/1.JNP.11.046023

Publication date:
2017

Document Version
Publisher's PDF, also known as Version of record

Link to publication from Aalborg University

Citation for published version (APA):
Skjølstrup, E. J. H., Søndergaard, T., Pedersen, K., & Pedersen, T. G. (2017). Optics of multiple grooves in metal: transition from high scattering to strong absorption. *Journal of Nanophotonics*, *11*(4), [046023]. https://doi.org/10.1117/1.JNP.11.046023

Optics of multiple grooves in metal: transition from high scattering to strong absorption

Enok J. H. Skjølstrup
Thomas Søndergaard
Kjeld Pedersen
Thomas G. Pedersen

Optics of multiple grooves in metal: transition from high scattering to strong absorption

Enok J. H. Skjølstrup, *Thomas Søndergaard, Kjeld Pedersen, and Thomas G. Pedersen**

Aalborg University, Department of Materials and Production, Aalborg East, Denmark

Abstract. This paper theoretically studies how the optics of multiple grooves in a metal change as the number of grooves gradually increased from a single groove to infinitely many arranged in a periodic array. In the case of a single groove, the out-of-plane scattering (OUP) cross section at resonance can significantly exceed the groove width. On the other hand, a periodic array of identical grooves behaves radically different and is a near-perfect absorber at the same wavelength. When illuminating multiple grooves with a plane wave, the OUP cross section is found to scale roughly linearly with the number of grooves and is comparable with the physical array width even for widths of many wavelengths. The normalized OUP cross section per groove even exceeds that of a single groove, which is explained as a consequence of surface plasmon polaritons generated at one groove being scattered out of the plane by other grooves. In the case of illuminating instead with a Gaussian beam and observing the limit as the incident beam narrows and is confined within the multiple-groove array, it is found that the total reflectance becomes very low and that there is practically no OUP. The well-known result for periodic arrays is thus recovered. All calculations were carried out using Green's function surface integral equation methods taking advantage of the periodic nature of the structures. Both rectangular and tapered grooves are considered. © *2017 Society of Photo-Optical Instrumentation Engineers (SPIE)* [DOI: 10.1117/1.JNP.11.046023]

Keywords: surface plasmons; diffraction and gratings; scattering theory; metal optics.

1 Introduction

Optics of grooves in metal has attracted attention due to their interesting scattering and absorption (ABS) properties. The optical cross sections of a single subwavelength ultrasharp or tapered groove in metal have been theoretically studied in detail in Ref. 1 establishing several fundamental results describing how the cross sections depend on the groove dimension. Here, it was found that the out-of-plane scattering (OUP) cross section can exceed the physical width of the groove in a broad wavelength interval. A periodic array of ultrasharp grooves is on the other hand found to give rise to broadband ABS, thus turning a shiny, highly reflecting surface into a black surface.[2,3] Thus, a single groove and a periodic array of grooves behave quite different, and in Ref. 1, it was suggested that the very low reflectance of the periodic array was due to mutual destructive interference between the scattered fields from the individual grooves. This hypothesis was recently tested in Ref. 4, where the optics of multiple ultrasharp grooves in metal was studied as the transition from one to infinitely many grooves. Surprisingly, it was found that the hypothesis was not correct when the incident field is a plane wave. The OUP cross section was found to scale approximately linear with the number of grooves and to be ~1.5 times larger than the physical width of the grooves even for widths of many wavelengths. Instead, it was found that when illuminating 20 grooves with a Gaussian beam entirely focused within the grooves, the reflectance is the same as for a periodic array illuminated by a plane wave.

*Address all correspondence to: Enok J. H. Skjølstrup, E-mail: ejs@mp.aau.dk

In this paper, we explore the same transition as in Ref. 4 but for rectangular and tapered (not ultrasharp) grooves and show that the same principles apply for these types of grooves when they are combined in an array of multiple grooves. For these types of grooves, the cross sections are found to be significantly large only for a narrow band of wavelengths,[5–8] and thus, the optical cross-section spectra are quite different from previous work.

An application for arrays of tapered grooves in metal is to use them in constructing broadband omnidirectional absorbers and angularly selective emitters.[9] As only p-polarized light will be efficiently absorbed in the grooves while s-polarized light will be almost perfectly reflected, an array of ultrasharp grooves can be applied as polarizers for ultrashort laser pulses.[10] As the rectangular and tapered grooves only absorb light for wavelengths close to the resonance, an application for those grooves is in selective thermal emitters,[11,12] which can be advantageous in thermophotovoltaics.[13,14]

The structure of interest in this paper is shown in Fig. 1(c), where the grooves can be either rectangular [Fig. 1(a)] or tapered [Fig. 1(b)]. The rectangular grooves have a depth of 500 nm and a width of 50 nm, whereas the tapered grooves have a depth of 350 nm, a top width of 100 nm, and a bottom width of 60 nm, where all the corners are rounded by a circle with a radius of 4 nm as in Ref. 5, implying that the top width of the rectangular grooves is 58 nm. The incident field in Fig. 1(c) is a normal Gaussian beam with beam waist radius w_0 centered at $x = x_0$ in the middle of the array of N identical grooves. There is a distance d between the grooves, and the total length of the groove array is denoted L. The beam waist radius is related to the array length by $w_0 = \gamma L/2$, where γ is a ratio parameter determining the width of the Gaussian beam. The schematic in Fig. 1(c) corresponds to $\gamma = 1$. The incident light can be either reflected, scattered upward, absorbed in the metal, or scattered into surface plasmon polaritons (SPPs), which are electromagnetic waves bounded to and propagating along the metal surface. As in Ref. 4 the magnetic field only has a z-component [$\mathbf{H}(r) = \hat{z}H(r) = \hat{z}H(x, y)$], and the structure is considered invariant in the z-direction, which implies that 2-D-calculations are performed. Gold is applied as the metal, and the dielectric constant of gold is from Ref. 15. The calculations are performed using the Green's function surface integral equation method (GFSIEM) as presented in Appendix B in Ref. 5. See Ref. 4 for a further description of how the matrix equation is constructed and solved using the iterative method GMRES.[16,17]

The paper is organized in the following way: Sec. 2 contains the case with a plane wave ($w_0 = \infty$) as the incident field, and here, extinction (EXT), scattering, and ABS cross sections are calculated for a structure of varying N, where the grooves are rectangular with the aforementioned dimensions. A Gaussian beam is used as the incident field in Sec. 3, where the grooves are still rectangular. Here, the beam waist radius is varied, and angular reflection spectra and total out-of-plane reflected power are calculated. In Sec. 4, the incident field is a plasmon and the reflectance, transmittance, and OUP is studied as a function of the number of grooves. In Sec. 5 the grooves are tapered, and here, both optical cross sections and reflectance as a function of wavelength are presented.
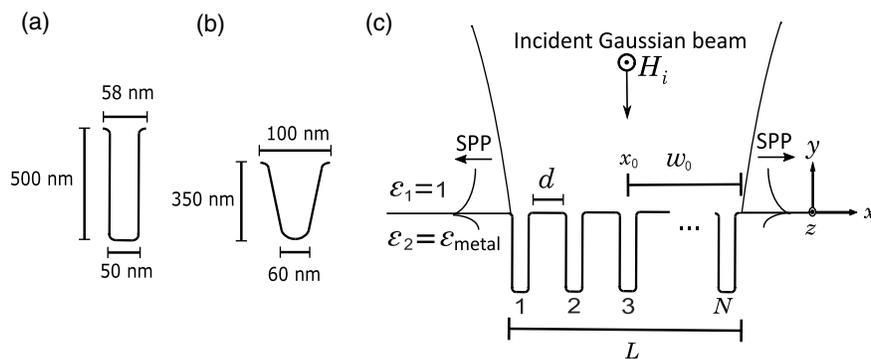

Fig. 1 (a) A rectangular groove, (b) a tapered groove, (c) schematic of N identical rectangular grooves in metal separated by the distance d. The incident field is a normal Gaussian beam with beam waist radius w_0 centered in the middle of the groove array ($x = x_0$).

2 Plane Wave as Incident Field

In this section, the incident field is a plane wave, which means that the beam waist radius w_0 in Fig. 1(c) tends to infinity. When light is incident on the multiple grooves, scattering occurs and some light is coupled into SPPs propagating along the metal surface away from the grooves, some light is scattered out of the plane, and some light is absorbed in the metal. EXT refers to the amount of power removed from the reflected beam due to scattering and ABS. The corresponding EXT, OUP, and SPP cross sections are obtained by normalizing the respective powers by the power per unit area of the incident light. The ABS cross section is given by the EXT cross-section minus the OUP and SPP cross sections. See Appendix B in Ref. 5 for a description of how the cross sections are calculated using the GFSIEM.

The rectangular shape of the grooves is found to give rise to a narrowband resonant behavior in all the cross sections.[5] For the particular dimensions of the grooves considered here, the cross sections of a single groove are found to be resonant at a wavelength of 660 nm as will later be shown in Fig. 5(a). Before multiple grooves are considered, it is chosen to study cross sections for a structure of only two grooves depending on the distance between them. It is chosen to fix the wavelength at $\lambda_0 = 660$ nm, and the EXT, OUP, and SPP cross sections are seen in Fig. 2 as a function of distance between the two grooves. All the cross sections are oscillating with certain extreme values to be explained. For the SPP cross section, the first minimum is found at $d = 260$ nm. With a top width of a single groove at 58 nm [see Fig. 1(a)], the period of the structure for this d is 318 nm, which equals a half plasmon wavelength, where $\lambda_{SPP} = \sqrt{(\varepsilon_1 + \varepsilon_2')/(\varepsilon_1 \varepsilon_2')}\lambda_0 = 635$ nm, and ε_2' is the real part of the metal dielectric constant ε_2.[18] Hence at $d = 260$ nm, the SPPs generated at the different grooves interfere destructively implying that the SPP cross section is practically 0. When this happens almost all of the scattered light is coupled out of the plane, as seen by the fact that the OUP cross section is a maximum at almost the same d for which the SPP cross section is minimized. When d increases toward a plasmon wavelength, plasmons generated at the different grooves interfere constructively implying that scattering into SPPs has a maximum, and at approximately the same d, both the OUP and EXT cross sections are minimized. At $d = 300$ nm, the EXT cross section has a maximum; at $d = 600$ nm, it has a minimum; therefore, it is chosen to consider these distances in the following. The inset in Fig. 2 shows the differential OUP cross section for $d = 600$ nm. Here, interference similar to a double slit predicts that destructive interference occurs at 60 deg and 120 deg, which is verified in the inset.[19]

For multiple grooves, the EXT, OUP, and ABS cross sections are seen at a wavelength of 660 nm in Fig. 3 when the distance d is 300 nm in (a) and 600 nm in (b). Especially in Fig. 3(a), the cross sections are almost linear functions of the number of grooves, while in Fig. 3(b) the linear behavior first begins after ~10 grooves. It is clearly seen that the cross sections in Fig. 3(a) are much larger than those in Fig. 3(b), and this large difference is not entirely caused by the fact that the EXT and OUP cross sections are smaller for $d = 600$ nm than for $d = 300$ nm according to Fig. 2. As will later be shown in Fig. 5(b) for $d = 600$ nm, the resonance wavelength is
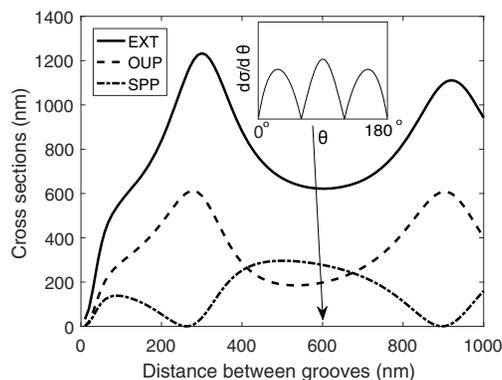

Fig. 2 EXT, OUP, and SPP cross sections for a structure of two grooves with varying distance d between the grooves. The inset shows the differential OUP cross section at $d = 600$ nm. The wavelength is 660 nm.
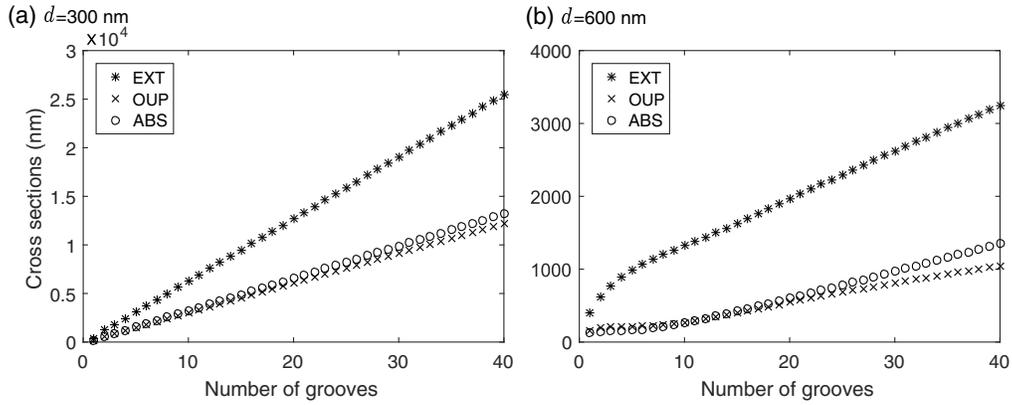
Fig. 3 EXT, OUP, and ABS cross sections at $\lambda = 660$ nm, where (a) $d = 300$ nm and (b) $d = 600$ nm.

blue-shifted from the 660 nm being the resonance wavelength of a single groove and furthermore a smaller peak occurs around 700 nm. Hence, when the wavelength is 660 nm, as is the case in Fig. 3, there is no resonance for $d = 600$ nm, which implies that the cross sections are much smaller compared with Fig. 3(a). For $N = 40$ grooves the OUP cross section is ~12 μm for $d = 300$ nm, and here, the total length of the groove array is $L \approx 14$ μm. However, the grooves themselves only occupy approximately one sixth of the length, as the distance d between the grooves is much larger than the groove width. The OUP cross section per groove is seen in Fig. 4, where again $d = 300$ nm in (a) and $d = 600$ nm in (b). In Fig. 4(a), the OUP cross section per groove converges to ~300 nm, which is ~0.85 times the groove period, but more than five times larger than a single groove width. For $d = 600$ nm, the OUP cross section for 40 grooves is ~1 μm as seen in Fig. 3(b), and the OUP per groove thus converges to ~25 nm as seen in Fig. 4(b). This much smaller cross section per groove is again due to the fact that for $d = 600$ nm the wavelength at 660 nm is not resonant.

The linear behavior of the EXT, OUP, and ABS cross section as a function of number of grooves was recently found for ultrasharp grooves in Ref. 4, where the OUP per groove was found to be ~1.5 times the groove period. In this study, the grooves had a wide opening at 240 nm in the top and a bottom width of only 0.3 nm with only $d = 10$ nm between the grooves. Furthermore, the reflectance of an infinite array of the same grooves illuminated by a plane wave was found in Ref. 2 to be 16% for this particular wavelength at 770 nm, and the extraordinary large OUP cross section for a structure consisting of 40 grooves was, therefore, a surprising and remarkable result. For the rectangular grooves considered in this paper, the OUP cross section per groove is thus comparable with Ref. 4, but with the difference that it is smaller than
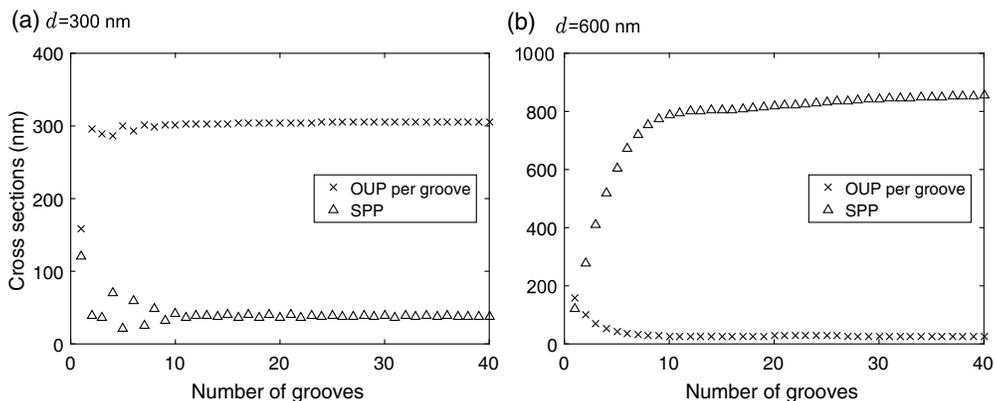
Fig. 4 SPP and OUP cross sections per groove at $\lambda = 660$ nm, where (a) $d = 300$ nm and (b) $d = 600$ nm.

the groove period (by the factor ≈ 0.85) but much larger than a single groove width (by the factor > 5).

The SPP cross section is shown by the triangles in Fig. 4 being a damped oscillatory function in Fig. 4(a) and an increasing function in Fig. 4(b). According to Fig. 2, the distance $d = 300$ nm is close to the minimum where the plasmons generated at different grooves interfere destructively resulting in a small SPP cross section. Another phenomenon that implies a small SPP cross section is the fact that a plasmon generated at one groove can be coupled out of the plane by another groove as examined in Refs. 20–22. This effect will be studied in detail in Sec. 4. In Fig. 4(b), the distance d is close to the maximum of SPP cross section according to Fig. 2. Here, plasmons generated at different grooves interfere constructively resulting in an overall increase in the total SPP cross section. Hence, if the purpose of the structure is to efficiently excite plasmons the groove period should be close to the plasmon wavelength as studied in Refs. 23 and 24. In addition, it was found in Refs. 25 and 26 that the dimensions of the individual grooves can be optimized in such a way that most of the incident light is excited into SPPs. Furthermore, the efficiency of SPP excitation from a single and multiple (but finite) rectangular grooves is studied in Ref. 27, showing that the SPPs can be excited with a significantly higher efficiency when more grooves are present.

While only a wavelength of 660 nm has been considered so far, the EXT cross section is seen as a function of wavelength for a structure consisting of 1, 5, 10, and 20 grooves in Fig. 5 for $d = 300$ nm in (a) and $d = 600$ nm in (b). Especially in Fig. 5(a), the EXT cross-section scales approximately linear with N for all considered wavelengths, and the same is found for the OUP and ABS cross sections (not shown). Here, the resonance wavelength has slightly changed from 660 nm for one groove into 657 nm for 20 grooves. This change in resonance wavelength is more pronounced in Fig. 5(b) where it is blue-shifted by ~ 30 nm compared with the spectrum for a single groove, but as N increases, the resonance wavelength slightly red-shifts again. As in Fig. 5(a) the EXT cross-section scales roughly linear with N at most wavelengths. However, in Fig. 5(b) the groove period is comparable with the wavelength, which implies that Rayleigh–Wood anomalies split the resonance wavelength into two peaks instead of one.[28–30] This splitting is more pronounced for $N = 20$ implying that the linear scaling of EXT with N fails for wavelengths around 700 nm for $N < 20$.

The same linear scaling of EXT cross section for many wavelengths was recently found in Ref. 4 for ultrasharp grooves, where the cross sections were large in a much broader wavelength interval. Based on this linear scaling for a specific groove dimension, and the study of the cross sections of a single groove for many different groove dimensions in Ref. 1, it was postulated in Ref. 4 that the linear scaling will also be valid for other groove dimensions, and Fig. 5(a) confirms this for a rectangular groove being a narrowband resonator.

As seen in Fig. 3, the OUP cross-section scales approximately linear with the number of grooves. To further study the out-of-plane scattering from multiple grooves, the differential OUP cross section is shown in Fig. 6 for a structure consisting of 1, 5, 10, and 20 grooves
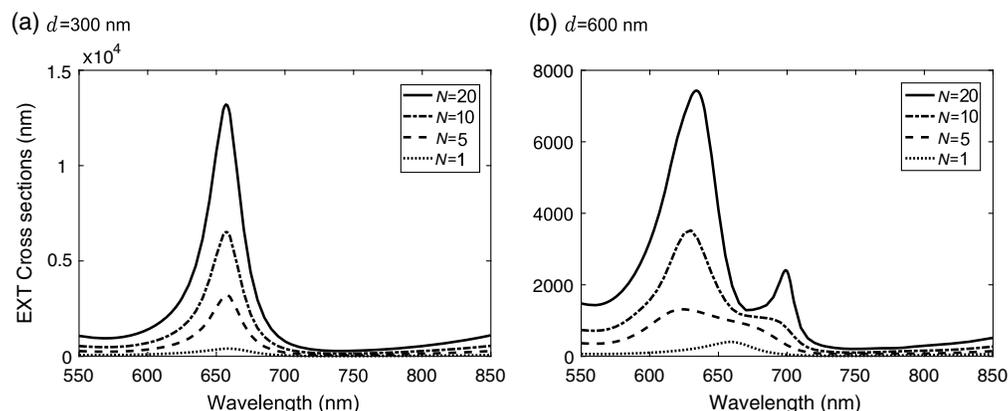
Fig. 5 EXT cross sections for 1, 5, 10, and 20 grooves as a function of wavelength, where (a) $d = 300$ nm and (b) $d = 600$ nm.
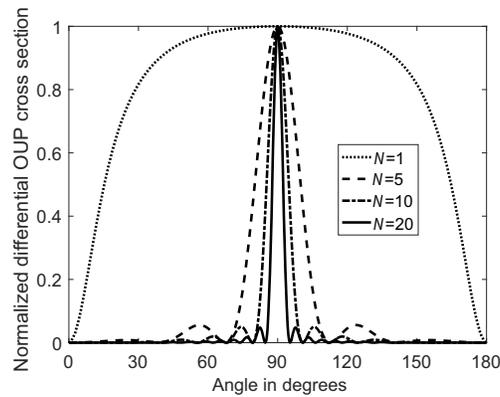
Fig. 6 Normalized differential OUP cross sections for 1, 5, 10, and 20 grooves for $\lambda = 660$ nm and $d = 300$ nm.

with $d = 300$ nm and $\lambda = 660$ nm. The differential cross sections have all been normalized such that they have a maximum of 1. When many grooves are present the angular distribution clearly becomes much more narrow. Notice that the OUP cross section is found by integrating the differential OUP cross section from 0 deg to 180 deg.

3 Gaussian Beam as Incident Field

In this section, the incident field is a Gaussian beam with beam waist radius $w_0 = \gamma L/2$ as shown in Fig. 1(c) for $\gamma = 1$. The same type of calculations as in Ref. 4 is performed, see for example, the appendix in Ref. 4 for a further explanation of the calculation of relevant terms.

3.1 Reflectance as a Function of Beam Waist Radius

First, it is studied how the incident field and reflected field depend on the ratio parameter γ, which determines the beam waist radius of the Gaussian beam. A structure consisting of 20 grooves with $d = 300$ nm between the grooves is considered, and the wavelength is chosen to be 660 nm. The incident power per angle is seen by the bright lines (blue online) in Fig. 7(a) for $\gamma = 0.5$ and 2, and even for such small γ the beam is still paraxial (meaning that $2\pi w_0/\lambda \gg 1$) as the structure has been chosen to be sufficiently wide such that this is achieved for $\gamma \geq 0.5$. It is clearly seen that a smaller γ implies that the angular distribution
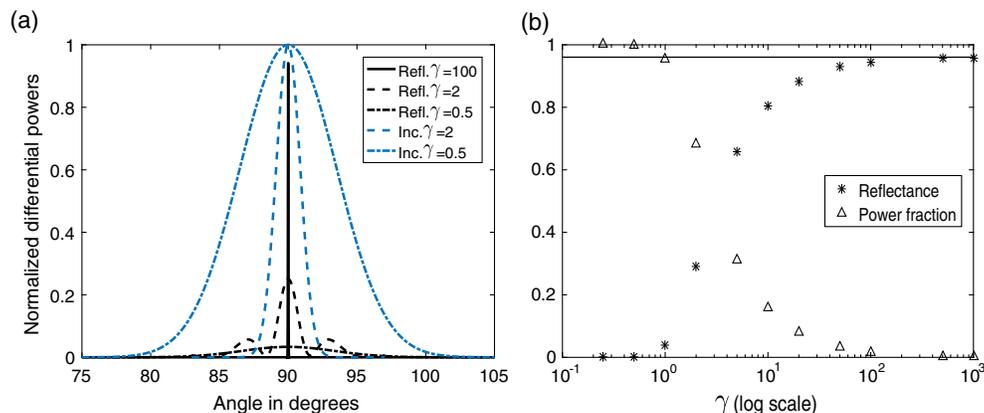
Fig. 7 (a) Normalized differential incident power for varying γ is seen by the bright lines (blue online) and the normalized differential reflected power in black at a wavelength of $\lambda = 660$ nm. (b) Reflectance and power fraction as a function of γ for 20 grooves at a wavelength of $\lambda = 657$ nm. The distance $d = 300$ nm in both (a) and (b).

is broader. The reflected power per angle is seen in black in the same figure when $\gamma = 0.5, 2$, and 100. For $\gamma = 100$, the incident field is so wide that it mostly hits the planar surface surrounding the grooves and the grooves themselves only marginally contribute. Therefore, the incident and reflected beams are almost the same, why only the reflected field is shown in Fig. 7(a), and it is very narrow in angular distribution as it behaves almost, such as a plane wave. The reflectance is found as the area under the black curve divided by the area under the corresponding blue curve and is found to be 0.03, 0.31, and 0.95 when $\gamma = 0.5, 2$, and 100, respectively. Hence, the reflectance strongly depends on γ since a high γ implies that the Gaussian beam also hits the planar surface and not entirely the grooves. This is found not to be the case for $\gamma \leq 0.5$, why in this case the calculated reflectance is entirely due to the grooves and not the surrounding planar surface.

The reflectance is thus calculated as a function of γ and is shown by the asterisks as in Fig. 7(b) for the same structure consisting of 20 grooves with $d = 300$ nm. Notice that the γ-axis in the figure is on a log scale.

As mentioned in Sec. 2, the resonance wavelength for the structure consisting of 20 grooves has slightly changed into 657 nm, why this wavelength has been used in Fig. 7(b) while 660 nm was the wavelength in Fig. 7(a). The reflectance is seen to converge for both small and large γ, where it converges to the proper reflectance, which is entirely due to the grooves when $\gamma \leq 0.5$ and converges to that of a flat gold surface when γ is large, as illustrated by the black horizontal line in the figure. The power fraction illustrated by the triangles in the same figure shows the geometric fraction of the incident power that actually hits the grooves. This fraction is practically 1 for $\gamma \leq 0.5$ and is practically 0 for $\gamma \geq 500$. Importantly, notice that the reflectance and power fraction converge for the same γ.
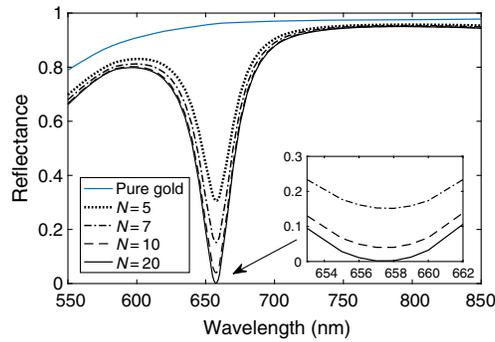
3.2 Reflectance as a Function of Number of Grooves

In this subsection, it is studied how the reflectance depends on the number of grooves for a fixed beam waist radius w_0, which is set to 1715 nm corresponding to $\gamma = 0.5$ for 20 grooves. In Fig. 8, the reflectance as a function of number of grooves is seen for $\lambda = 657$ nm and converges to practically 0 when 20 grooves are present. Thus, it is found that 20 grooves are sufficient to obtain the same reflectance as a structure consisting of infinitely many grooves. As in Fig. 7(b), the triangles show the power fraction and it converges to 1 when 20 grooves are present as was also observed in Fig. 7(b). Hence, Fig. 8 shows that the reflectance converges to the proper reflectance of the grooves when all the incident light hits the groove array. The same result was obtained in Ref. 4 for ultrasharp grooves.

Whereas Fig. 8 only considered $\lambda = 657$ nm the reflectance as a function of wavelength is seen in Fig. 9 for 5 to 20 grooves, where $d = 300$ nm and $w_0 = 1715$ nm. The reflectance of the structure consisting of 20 grooves is found to be the same as for a periodic array of the same grooves illuminated by a plane wave as studied in Ref. 5, and the same result was found in Ref. 4 for ultrasharp grooves. The reflectance is shown for 5, 7, 10, and 20 grooves and is low, close to the resonance wavelength and comparable with that of pure gold for longer wavelengths. Here, more grooves imply that the reflectance at resonance becomes lower as was also shown in Fig. 8,
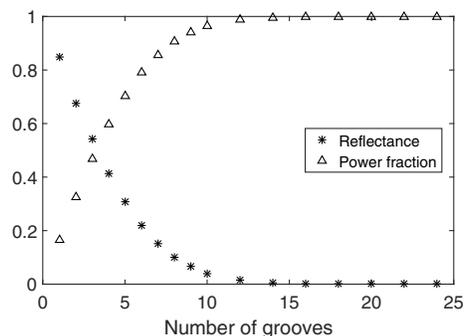
Fig. 8 Reflectance and power fraction as a function of number of grooves for a fixed beam waist $w_0 = 1715$ nm. The wavelength is 657 nm and $d = 300$ nm.

Fig. 9 Reflectance as a function of wavelength for 5 to 20 grooves, with $d = 300$ nm and $w_0 = 1715$. Inset shows the reflectance in a smaller wavelength interval.

but off resonance the reflectance is almost independent of the number of grooves. The inset in Fig. 9 shows the reflectance for a smaller wavelength interval close to the resonance wavelength, and here it is possible to see the difference in reflectance between 10 and 20 grooves. It is remarkable that the reflectance of 20 grooves when illuminating with a Gaussian beam becomes practically 0, when the same groove structure illuminated with a plane wave has a very large OUP cross section as observed in Sec. 2. The same kind of result was found in Ref. 4 for ultra-sharp grooves, and there, it was postulated to be valid for other groove dimensions as well, and Fig. 9 confirms this for rectangular grooves.

3.3 Energy Transportation

As in Ref. 4, the energy transportation is investigated based on the time-averaged Poynting vector $\langle \mathbf{S} \rangle = 1/2 \operatorname{Re}(\mathbf{E} \times \mathbf{H}^*)$, where $\mathbf{E}$ and $\mathbf{H}$ are the complex electric and magnetic field, respectively, and where * denotes complex conjugation. The interpretation of the Poynting vector is that it points in the direction of the power flow with a magnitude describing the power flow per unit area.[18] Figure 10 shows the magnitude of the time-averaged Poynting vector when a Gaussian beam with ratios of 0.5, 1, 2, and ∞ (plane wave) is incident on a structure consisting of 20 grooves with $d = 300$ nm between the grooves and with a wavelength of 660 nm. The black horizontal lines in the figure illustrate the length of the groove array. When $\gamma = 0.5$ the
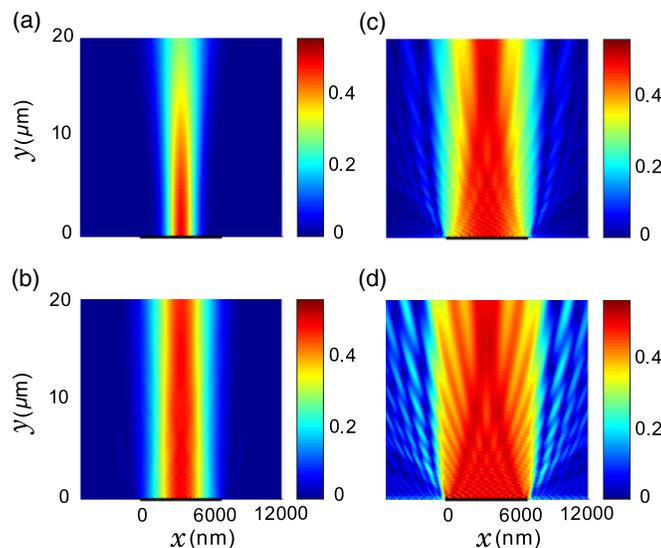

Fig. 10 (Color online) Magnitude of time-averaged Poynting vector when a Gaussian beam is incident on a structure consisting of 20 grooves at a wavelength of 660 nm with $d = 300$ nm. The horizontal black lines denote the groove array and the ratios are (a) $\gamma = 0.5$, (b) $\gamma = 1$, (c) $\gamma = 2$, and (d) $\gamma = \infty$ (plane wave).

incident field is entirely focused within the grooves [see Fig. 7(b)], which implies that there is almost no light scattered out of the plane. This is clearly observed in Fig. 10(a), where the magnitude of the Poynting vector is zero for all other positions than right above the groove array. When γ increases, more light is scattered out of the plane as shown in Figs. 10(b)–10(d). When the incident field is a plane wave, as shown in Fig. 10(d), most of the incident light hits the planar surface surrounding the grooves where they experience almost total reflectance as pure gold is almost a perfect mirror at this wavelength. Hence, far outside the grooves, the net power flow is very low. The angular distribution of the scattered field is broader for $\gamma = \infty$ than for $\gamma = 2$ [Fig. 10(c)], which was also partly shown in Fig. 7(a) as the oscillations in differential powers for angles deviating from 90 deg.

4 Plasmon as Incident Field

In this section, we consider an SPP being incident on multiple rectangular grooves with $d = 300$ nm between the grooves. A schematic of this situation is shown in Fig. 11(a), where the SPP is incident from left, thus it can be reflected, transmitted, scattered out of the plane, or absorbed. The reflectance, transmittance, and OUP of an SPP incident on multiple rectangular grooves have previously been considered in Refs. 20 and 21 whereas the case of a single groove or ridge of different shapes was considered in Ref. 22 and the case of a rectangular hole in Ref. 31. The case of short- and long-range SPPs of thin-metal films being incident on a rectangular metal nanostrip forming a gap-plasmon resonator together with the metal film has also been considered.[32]

Figure 11(b) shows the reflectance, transmittance, and OUP for a plasmon being incident on a single groove as a function of wavelength. Like in Figs. 5(a) and 9(a), clear resonant behavior is observed with a dip in transmittance relatively close to the resonant wavelength at 657 nm. The fact that a part of the incident plasmon is scattered out of the plane at resonance serves as a qualitative explanation of why the OUP per groove is higher for multiple grooves compared with the single groove case as was observed in Fig. 4(a). Figure 11(c) shows the reflectance, transmittance, and OUP, as a function of number of grooves at $\lambda = 657$ nm. The plasmon transmittance through one groove is almost 50% but decreases as more grooves are present while the scattering and ABS level increase. When 10 grooves are present less than 1% of the incident light is transmitted, and therefore, all three curves remain constant hereafter. For ultrasharp grooves, it was found in Ref. 4 that still 5% of the incident light was transmitted through a structure consisting of 20 grooves (at $\lambda = 770$ nm). Hence, the array of rectangular grooves blocks the light of an incident plasmon better compared with an array of ultrasharp grooves. Notice that the plasmon reflectance is highest when two grooves are present, which is due to the fact that the distance between the grooves is roughly a half wavelength, thus the reflected light from the two
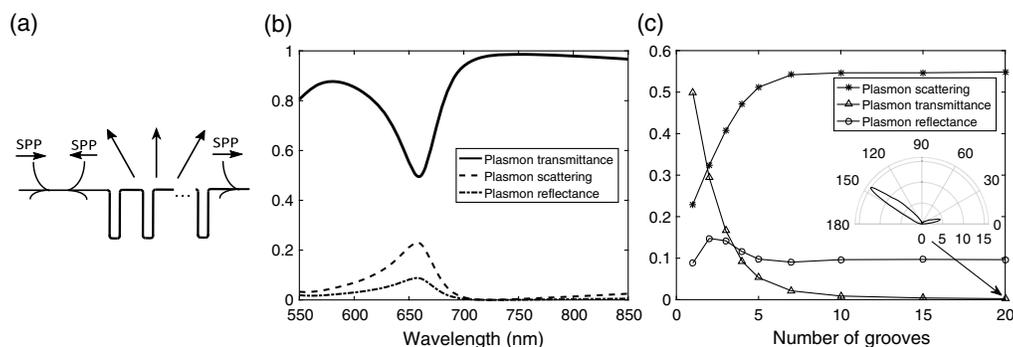
Fig. 11 (a) Schematic of an SPP wave incident from left on multiple rectangular grooves. The incident plasmon can be reflected, transmitted, or scattered out of the plane. (b) Plasmon reflectance, transmittance, and scattering in the case of one groove as a function of wavelength. (c) Plasmon reflectance, transmittance, and scattering as a function of number of grooves for $\lambda = 657$ nm and $d = 300$ nm. Inset shows normalized differential power for a structure consisting of 20 grooves.

(a)

(b)
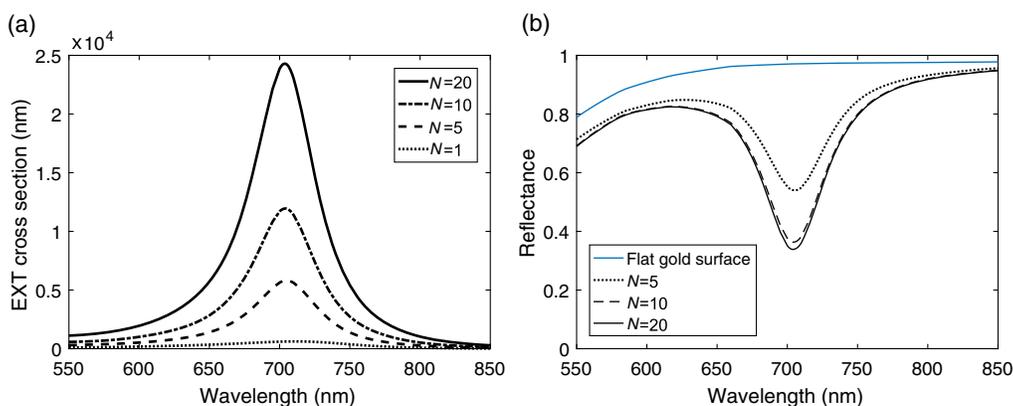
Fig. 12 (a) EXT cross section as a function of wavelength for 1, 5, 10, and 20 tapered grooves. (b) Reflectance as a function of wavelength for 5, 10, and 20 tapered grooves with $w_0 = 1925$ nm. The distance d between the grooves is 300 nm in both (a) and (b).

grooves interferes constructively resulting in a higher plasmon reflectance. When more grooves are present, multiple reflections within the groove array imply that the plasmon reflectance decreases. The inset in Fig. 11(c) shows a polarplot of the normalized differential power when 20 grooves are present showing that most of the scattered light is actually scattered obliquely backward at an angle of approximately 150 deg. The plot has been normalized such that integrating the differential power from 0 deg to 180 deg gives 0.55, which is the plasmon scattering for 20 grooves.

5 Tapered Grooves

Until now rectangular grooves have been examined as shown in Fig. 1(a). In this section, tapered grooves are considered with a depth of 350 nm, a top width of 100 nm, and a bottom width of 60 nm as seen in Fig. 1(b). In Ref. 5, tapered grooves are found to give rise to broader resonances compared with rectangular grooves, which can be understood in terms of the resonator formalism presented therein. The tapered grooves are studied here following the same procedure as for the rectangular grooves studied in Secs. 2 and 3. Thus first two grooves are studied, and the cross sections found as a function of distance between the grooves. The result is found to be very similar to Fig. 2 and with approximately the same d giving rise to the extrema. The EXT cross section as a function of wavelength is seen in Fig. 12(a) for a structure consisting of 1, 5, 10, and 20 grooves with $d = 300$ nm between the grooves, where the resonance wavelength is 704 nm. The spectra are quite similar to those of the rectangular grooves in Fig. 5(a) but with a broader resonance. Again the EXT cross section scales almost linear with the number of grooves for the considered wavelengths. The reflectance of the same structure when illuminating with a Gaussian beam is seen in Fig. 12(b) and follows the same principles as the rectangular grooves in Fig. 9. Here, the beam waist radius w_0 has been fixed at 1925 nm, which here corresponds to $\gamma = 0.5$ for a structure consisting of 20 grooves. Again the reflectance of the structure consisting of 20 grooves is the same as for a periodic array of the same grooves illuminated by a plane wave. Here, the reflectance at resonance is 0.34 even when 20 grooves are present, illustrating that the grooves have to be sufficiently narrow in order for the reflectance at resonance to be very low. Hence for the tapered grooves considered here, the resonance is broader, and it is not possible to achieve perfect ABS as for rectangular grooves.

6 Conclusion

The optics of multiple rectangular and tapered grooves in metal has been studied theoretically to examine the transition from a single groove to infinitely many grooves arranged in a periodic array. When the incident field is a plane wave the OUP cross section depends approximately

linearly on the number of grooves, a result that was also recently found for multiple ultrasharp grooves. The OUP cross section per groove is comparable with the groove period even though the scattering structure has a width of many wavelengths. Furthermore, the OUP cross section per groove is higher than for a single groove, which is explained by the fact that an SPP generated in one groove can be scattered out of the plane by other grooves, and this is supported by studying the reflectance, transmittance, and OUP when an SPP is incident on multiple grooves. A structure consisting of infinitely many grooves in a periodic array illuminated by a plane wave has a very low reflectance at resonance, but this is not due to destructive interference occurring between the scattered fields of different grooves. Instead, a narrow Gaussian beam focused entirely within the grooves has to be used as the incident field in order for the reflectance of multiple grooves to be the same as for an infinite array of grooves illuminated by a plane wave.

When the distance between the rectangular grooves is 300 nm a structure consisting of 20 grooves is found to be a near-perfect absorber for wavelengths close to 657 nm while it, for longer wavelengths, is a nearly perfect mirror. When the distance between the grooves increases to 600 nm the reflectance is found to be close to that of pure gold independent on the number of grooves in the structure. For tapered grooves, the resonance is broader, but the minimal reflectance is found to be 0.34 even when 20 grooves are present, and the tapered grooves considered here can, therefore, not be used as a perfect absorber.

Acknowledgments

References

1. T. Søndergaard and S. I. Bozhevolnyi, "Optics of a single ultrasharp groove in metal," *Opt. Lett.* **41**, 2903–2906 (2016).
2. T. Søndergaard et al., "Plasmonic black gold by adiabatic nanofocusing and absorption of light in ultra-sharp convex grooves," *Nat. Commun.* **3**, 969 (2012).
3. T. Søndergaard and S. I. Bozhevolnyi, "Theoretical analysis of plasmonic black gold: periodic arrays of ultra-sharp grooves," *New J. Phys.* **15**, 013034 (2013).
4. E. J. Skjølstrup and T. Søndergaard, "Optics of multiple ultrasharp grooves in metal," *J. Opt. Soc. Am. B* **34**, 673–680 (2017).
5. A. Roberts et al., "Light extinction and scattering from individual and arrayed high-aspect-ratio trenches in metals," *Phys. Rev. B* **93**, 075413 (2016).
6. J. L. Perchec et al., "Why metallic surfaces with grooves a few nanometers deep and wide may strongly absorb visible light," *Phys. Rev. Lett.* **100**, 066408 (2008).
7. F. Pardo et al., "Light funneling mechanism explained by magnetoelectric interference," *Phys. Rev. Lett.* **107**, 093902 (2011).
8. J. Guo, Z. Li, and H. Guo, "Near perfect light trapping in a 2D gold nanotrench grating at oblique angles of incidence and its application for sensing," *Opt. Express* **24**, 17259–17271 (2016).
9. C. Argyropoulos et al., "Broadband absorbers and selective emitters based on plasmonic brewster metasurfaces," *Phys. Rev. B* **87**, 205112 (2013).
10. E. Skovsen et al., "Plasmonic black gold based broadband polarizers for ultra-short laser pulses," *Appl. Phys. Lett.* **103**, 211102 (2013).
11. J. Greffet et al., "Coherent emission of light by thermal sources," *Nature* **416**, 61–64 (2002).
12. H. Miyazaki et al., "Thermal emission of two-color polarized infrared waves from integrated plasmon cavities," *Appl. Phys. Lett.* **92**, 141114 (2008).
13. T. Bauer, *Thermophotovoltaics—Basic Principles and Critical Aspects of System Design*, 1st ed., Springer Verlag, Berlin (2011).
14. H. Sai and H. Yugami, "Thermophotovoltaic generation with selective radiators based on tungsten surface gratings," *Appl. Phys. Lett.* **85**, 3399–3401 (2004).

15. P. Johnson and R. Christy, "Optical constants of the noble metals," *Phys. Rev. B* **6**, 4370–4379 (1972).

16. R. Barrett et al., *Templates for the Solution of Linear Systems: Building Blocks for Iterative Methods*, 2nd ed., SIAM, Philadelphia (1994).

17. Mathworks, "GMRES," https://se.mathworks.com/help/matlab/ref/gmres.html (29 June 2017).

18. L. Novotny and B. Hecht, *Principles of Nano-Optics*, 2nd ed., Cambridge University Press, Cambridge (2012).

19. H. D. Young, R. A. Freedman, and A. L. Ford, *University Physics with Modern Physics*, 13th ed., Pearson, San Francisco (2012).

20. F. López-Tejeira, F. J. García-Vidal, and L. Martín-Moreno, "Scattering of surface plasmons by one-dimensional periodic nanoindented surfaces," *Phys. Rev. B* **72**, 161405 (2005).

21. G. Brucoli and L. Martín-Moreno, "Effect of depth on surface plasmon scattering by sub-wavelength surface defects," *Phys. Rev. B* **83**, 075433 (2011).

22. A. Y. Nikitin, F. López-Tejeira, and L. Martín-Moreno, "Scattering of surface plasmon polaritons by one-dimensional inhomogeneities," *Phys. Rev. B* **75**, 035129 (2007).

23. C. Ropers et al., "Grating-coupling of surface plasmons onto metallic tips: a nanoconfined light source," *Nano Lett.* **7**, 2784–2788 (2007).

24. I. P. Radko et al., "Efficiency of local surface plasmon polariton excitation on ridges," *Phys. Rev. B* **78**, 115115 (2008).

25. P. Lalanne et al., "A microscopic view of the electromagnetic properties of sub-λ metallic surfaces," *Surf. Sci. Rep.* **64**, 453–469 (2009).

26. B. Wang and P. Lalanne, "Surface plasmon polaritons locally excited on the ridges of metallic gratings," *J. Opt. Soc. Am. A* **27**, 1432–1441 (2010).

27. S. de la Cruz et al., "Compact surface structures for the efficient excitation of surface plasmon-polaritons," *Phys. Status Solidi B* **249**, 1178–1187 (2012).

28. T. Søndergaard et al., "Extraordinary optical transmission with tapered slits: effect of higher diffraction and slit resonance orders," *J. Opt. Soc. Am. B* **29**, 130–137 (2012).

29. A. A. Maradudin et al., "Rayleigh and wood anomalies in the diffraction of light from a perfectly conducting reflection grating," *J. Opt.* **18**, 024004 (2016).

30. U. Fano, "The theory of anomalous diffraction gratings," *J. Opt. Soc. Am.* **31**, 213–222 (1941).

31. H. Liu and P. Lalanne, "Microscopic theory of the extraordinary optical transmission," *Nature* **452**, 728–731 (2008).

32. T. Søndergaard, V. Siahpoush, and J. Jung, "Coupling light into and out from the surface plasmon polaritons of a nanometer-thin metal film with a metal nanostrip," *Phys. Rev. B* **86**, 085455 (2012).

Biographies for the authors are not available.